

Chapter 2

From Multichannel ECG to Wireless Body Sensors

Abstract A more detailed description of multichannel electrocardiography and the differential lead aims to clarify why the multichannel ECG opens a path towards implementation of wireless wearable sensors. Several ways of how the differential lead could be used for heart rhythm monitoring are shown with options for analysis and interpretation of sensor ECG measurements. Finally, the most important vital signs that could be provided by a multifunctional body sensor are presented.

2.1 Multichannel ECG

The body potentials can be measured simultaneously in many positions on the body, e.g., up to 300, by a multichannel ECG. However, such devices have been regarded as non-practical for clinical use because of their complexity, related to the burden of connection wires and electrodes, and because of complex analysis of a huge amount of acquired ECG data. On the other hand, a single-channel body ECG sensor [1] still represents a viable solution for the detection of many cardiac problems, including arrhythmias and conduction abnormalities.

A path from a multichannel ECG to a multifunctional sensor is described in more detail in the rest of this chapter. The multichannel electrocardiography (MECG) is an extension of the conventional electrocardiography. It is aimed at refining the non-invasive characterization of cardiac activity. Increased spatial sampling on the body surface provides more information on potentials generated by the heart [2, 3]. An instructive method for representing MECG signals is the body surface mapping (BSM) [4]. Such a representation can be given with isocontours, e.g. isopotential contours, in which case the map shows the body surface potential at a specific moment, or isointegral contours, in which case the map shows the distribution of the sum of potentials over a specified time interval (QRS, ST 40, etc.), or similar.

Various MECG systems have been used for deriving BSMs, with the number of electrodes ranging from 10 to 300 [5, 6]. The result of an MECG measurement are time series of sampled body surface potential differences, encapsulating the data collected by all the electrodes at each sampling time. These potentials can be presented by a BSM that visualizes, by isocontours, the interpolated MECG measurements.

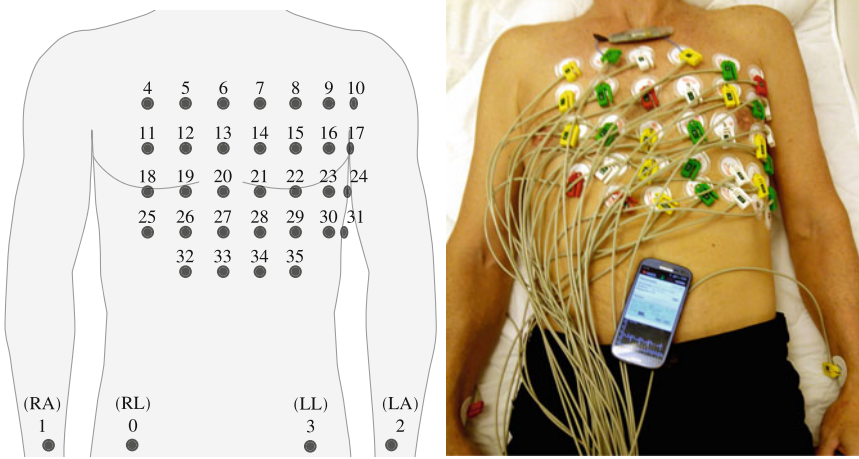


Fig. 2.1 Placing and numbering of 35 MECG electrodes (*left*) and an actual MECG system during a measurement with an ECG sensor in the top row (*right*)

The MECG measurements constitute a powerful research tool, because the redundant data can be used to validate findings, particularly in the cases when the interpretation of the conventional 12-lead ECG is not obvious. Such cases are, for example, when the signals from the electrodes are disturbed, or if the spatial variability of the heart parameters has to be examined [7, 8].

We have developed a custom-designed MECG device with 35 electrodes already in the 1990s [9] and have later acquired notable experiences with the acquisition of MECG measurements under different circumstances in laboratories and hospitals. The body potentials are measured as 32 unipolar leads referenced to the WCT, with electrodes placed on the thorax, and as standard 3 bipolar leads (I, II, III) with the electrodes placed on the limbs, i.e., one on each arm and one on the left leg. The right leg electrode (electrode 0) was also used for a ground reference. Equidistant positioning of the electrodes on the thorax is mostly used, but the MECG device allows also for a different positioning, if required. The equidistant positioning is often preferred because it enables simple BSM generation in which the measured potential differences from the electrodes are used directly, without a complicated weighted interpolation.

The preferred positioning and numbering of the 35 MECG electrodes is schematically shown in the left part of Fig. 2.1. The MECG system, during a measurement, is shown in the right part of Fig. 2.1. Note that an early prototype of the ECG sensor is connected in parallel with the MECG electrodes 5 and 7. The measured sensor ECG is shown on the smartphone. Further details on this particular MECG device can be found in [10].

As explained previously, the MECG measurements are values of local body surface potentials referenced to a selected reference point, e.g. the WCT, or alternatively the potential differences between two electrodes, e.g. standard bipolar leads, or also a

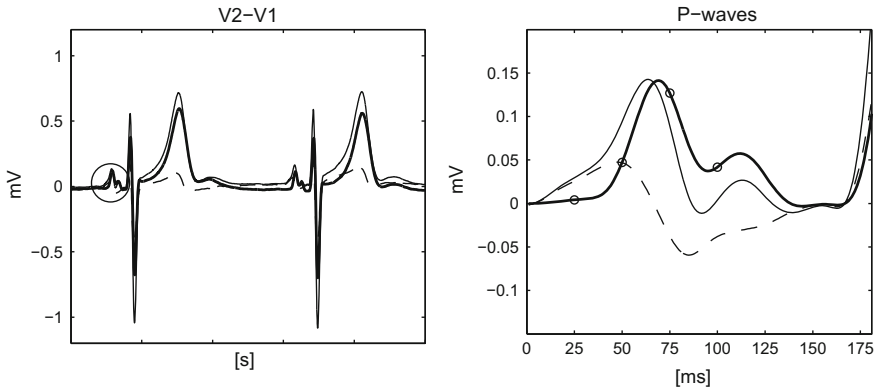


Fig. 2.2 Simultaneous measurements of the standard V1 (*dashed line*) and V2 (*solid line*) leads and the differential lead V2-V1 (*bold line*) for two consecutive beats (*left*), and a magnified PR interval of the first beat (*right*)

differential lead between two nearby MEEG electrodes. An example of two MEEG signals from the electrodes 12 and 14, and the differential lead signal from these electrodes, are shown in Fig. 2.2. Note that the MEEG electrodes 12 and 14, as numbered in the left part of Fig. 2.1, can be used as an approximation of the standard leads V1 and V2. The signals shown in Fig. 2.2 were captured simultaneously with 1000 samples per second and filtered by a 50 Hz low-pass filter.

According to the explanation in Chap. 1 and Fig. 1.5, the difference V2-V1 is the differential lead or the ECG that can be measured by a body sensor with its electrodes positioned on the standard places of the V1 and V2 electrodes. The magnified PR interval from the first beat, marked with a circle in the left part of Fig. 2.2, is shown in the right part of Fig. 2.2. The P-wave was selected because its analysis is crucial for the study of the heart rhythm. The measurement confirms the high fidelity of the ECG. Note that the scale of the right graph is larger than the scale of the left graph for better reproduction of the P-waves morphology. The samples at 25, 50, 75 and 100 ms after the start of the atrial depolarization, i.e., the onset of the P wave, are marked with small circles.

It can be seen that the P wave in the differential lead has similar timing for both standard leads. As explained, the differential lead represents the difference V2-V1. Therefore, it indicates the local gradient of the potential field between the standard leads. Comparing the P wave signals of the V1 and V2 leads (thin curves) with the P wave signal from the differential lead (bold curve), several interesting facts can be noticed. The amplitude of the P wave signal from the differential lead at 25 ms is close to zero, because the leads V1 and V2 are on the same potential at these moments. The peak of the P wave from the differential lead near 75 ms is slightly shifted to the right, compared to the P wave from V2 lead, because of the negative potential at V1. The P wave from the differential lead at 100 ms is larger than the P waves from the V1 and V2 leads, again because of the negative signal on V1. We can suspect that

the information from the differential lead is more local than the information obtained from the standard leads, which could help in the identification of local phenomena in the heart, e.g., focus areas for atrial [11] or ventricular premature beats [12]. This hypothesis is more formally supported in Chap. 5.

2.2 Body Surface Maps

An alternative view on MECG signals can be presented with BSMs. Four examples of isopotential BSMs, obtained from the presented MECG setup in Fig. 2.1, and for the same measurement setup as in Fig. 1.5, are shown in Fig. 2.3, again for 25 and 50 ms (upper two plots) and for 75 and 100 ms (lower two plots) after the start of atrial depolarization. The difference between two neighboring contours is 5 μV . The MECG electrode positions are marked with small circles. The ECG of the three missing MECG electrodes from the lowest horizontal line (in Fig. 2.1) have been extrapolated from signals of the neighboring electrodes, just to obtain a rectangular 7×5 grid. For example, the signal of the missing electrode in the position (1,1) was obtained by averaging the signals of electrodes positioned in (1,2) and (2,1), which are numbered as 25 and 32, respectively. The approximated standard positions of V1 and V2, i.e. the MECG electrodes 12 and 14, are shown for comparison in the positions (2,5) and (4,5), respectively.

Since the differential lead is defined as a potential difference from two proximal points on the BSM, we can treat the measurement as a spatial derivative of the BSM, which can be obtained by the gradient of the measured MECG field of potentials:

$$\nabla BSM(x, y) = \frac{\partial BSM}{\partial x} \mathbf{i} + \frac{\partial BSM}{\partial y} \mathbf{j} \quad (2.1)$$

where \mathbf{i} and \mathbf{j} are unit vectors in the x and y dimensions. The BSM gradient can be visualized by vectors that indicate the amount of the expected signal between two neighboring MECG electrodes, which is equivalent to the potential differences between the neighboring MECG electrodes. The gradients of the BSM potentials from Fig. 2.3 are shown in Fig. 2.4. This visualization can be used to help positioning the ECG sensor on an optimal place. A criterion for the selection of the best neighboring MECG electrodes that provide sufficient ECG signal could be the presence of large spatial derivatives throughout the PR interval. The component of the sum of vectors from Fig. 2.4, which is aligned with an imaginary straight line that connects both sensor electrodes, is the potential difference measured by the ECG sensor. We see that by this criterion, a good position is between the MECG electrodes 12 and 14, i.e., between the standard leads V1 and V2, which are also among the closest to the heart atria. There are also several other good positions, all in the vicinity of the heart.

Despite of their informative dominance, BSMs have not become a part of standard clinical procedures, because of the high complexity of MECG setup and because of

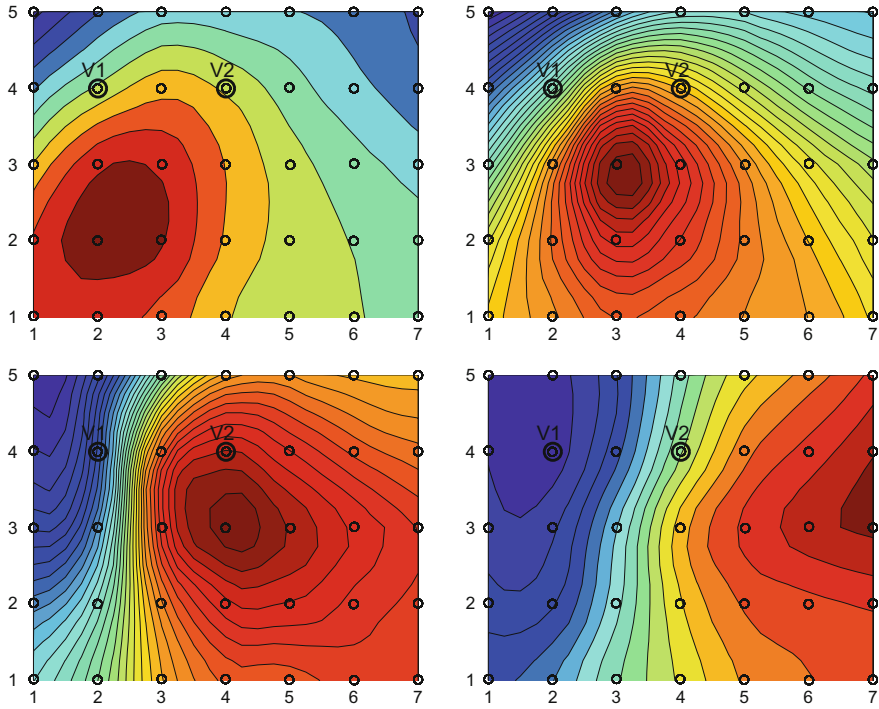


Fig. 2.3 Isopotential BSMs depicting the moments at 25 and 50 ms (*above*), and 75 and 100 ms (*below*), after the start of atrial depolarization

practical complications with many wired body electrodes. Furthermore, the interpretation of the BSM data is complex and still a part of ongoing research. However, in the era of high-performance ICT technologies and wireless communication, this situation may change if wireless and computerized MEG systems appear. In particular, a potential benefit from the analysis of BSM data is the provision of accurate methodologies for non-invasive analysis of the heart activity. With the advent of computers, powerful automatic algorithms can be implemented to process the measurements online, offering to medical practitioners more reliable and more specific diagnoses than the conventional 12-lead ECG.

From our early experience with the development of MEG systems and from MEG measurements, we have learned that the potential differences from closely positioned body electrodes provide a complete information about the heart rhythm. Furthermore, a “closer look” on the heart through the differential lead can elucidate more specific heart diagnoses. It is also evident that the signal-to-noise ratio decreases with the increase of the electrodes’ proximity, which can result in lower accuracy of the measured ECG. Nevertheless, the breakthrough idea that enables the implementation of a small and wireless ECG sensor comes from our previous work in the area of MEG. We expect that in the near future, numerous online mHealth systems [13]

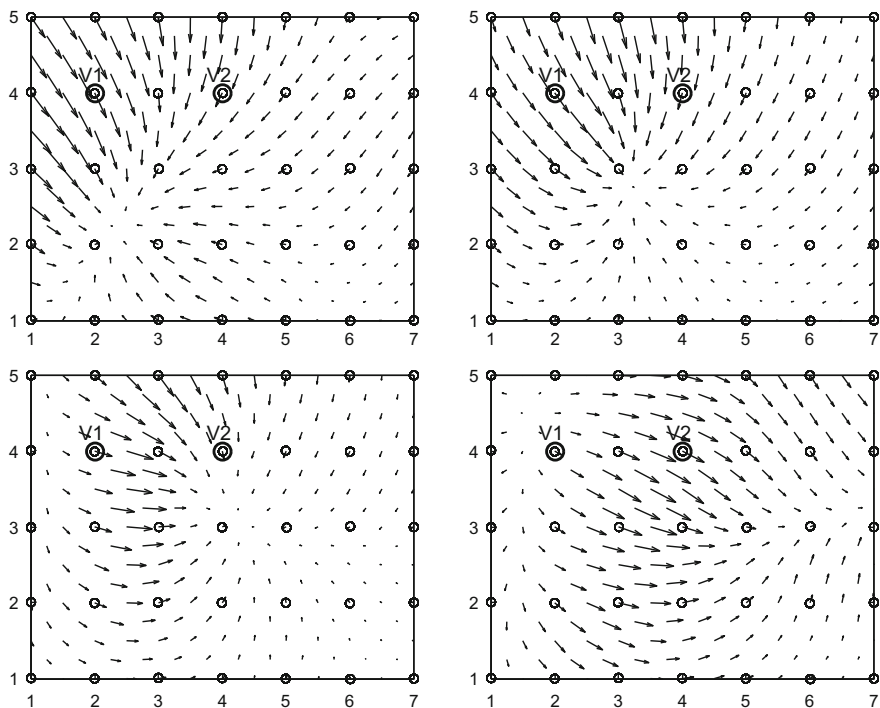


Fig. 2.4 Gradients of the isopotential BSMs from Fig. 2.3 at 25 and 50 ms (*above*), and 75 and 100 ms (*below*), after the start of atrial depolarization

will use a minimized set of sensors, with potentially personalized positioning, that will be able to synthesize the conventional 12-lead ECG. A more detailed discussion about this topic is given in Chap. 5.

2.3 Wireless Body Sensor

2.3.1 Prerequisites for Body Sensor Design

There are two major difficulties that have to be overcome to continuously and wirelessly measure electrical bio-potentials on a human body:

1. The bio-potentials reflect activities of living tissues, which are changing at intervals often much shorter than a single second. To get their reliable digital representation, the signals must usually be sampled more than hundred times per second. One has to either process the data measurements on the sensor or wirelessly transmit a large amount of streamed data to a more complex assisting device. In both

cases, a significant energy is consumed on the sensor because of the need for high computation or communication. Consequently, both implementation options limit the sensor autonomy. Usually, developers have to find an optimal combination between local computation and communication.

2. The electric potential differences cannot be measured between “wireless” points on the body; a conductive path (wire) is required between them for measuring the difference in the electric potential, i.e., the voltage. If the two connected points are close enough, they can be packed, together with the corresponding electronics, into a single body sensor.

A further goal of sensor developers has to be a technological solution for a medical grade multifunctional wireless body sensor with small dimensions (e.g., 10 cm) and a small weight (e.g., 15 g), which allows for unobtrusive use during every-day activities, exhaustive physical work, sleep and sports. The body sensor should be formatively designed so that it resembles an ornament, to make it more appealing to the users. However, it must also be fixed on the body reliably, and be taken on and off without damaging the skin. The distance between the electrodes should be small, but still sufficient to guarantee the signal-to-noise ratio required for accurate measurements. As said, the sensor should be multifunctional because users are ready to wear just a few sensors, ideally a single one, at a time. It should sense vital physiological signs (ECG, muscular activity, respiration, etc.) and relevant environmental parameters (acceleration, light intensity, temperature, etc.).

Finally, the body sensor should have a long autonomy, e.g., one week or more, a low-power wireless connection to a smartphone or some other personal assisting device, and should be accompanied with a simple software for the marking of cardiac-related events, for the generation of ECG reports, and for the visualization and interpretation of measurements. Regarding the medical grade, a moderate resolution of the ECG and eventual other signals should be suitable for long-term personal cardiac activity monitoring, as well as for clinical use. The fusion of the acquired data, physiological and environmental, should increase the interpretability of the measurements and allow for ambient intelligence. The sensor should support solutions to every-day problems of the medical personnel in hospitals, health clinics, homes for the elderly and health resorts.

As an example, a multifunctional body sensor prototype that fulfills most of the above listed design goals and requirements is shown in the left part of Fig. 2.5. Through co-design by engineers, patients and medical practitioners, the prototype has been upgraded into the near-to-market version shown in the right part of Fig. 2.5. Note that the body sensor is small, light and flexible, and therefore minimally obtrusive for the users.

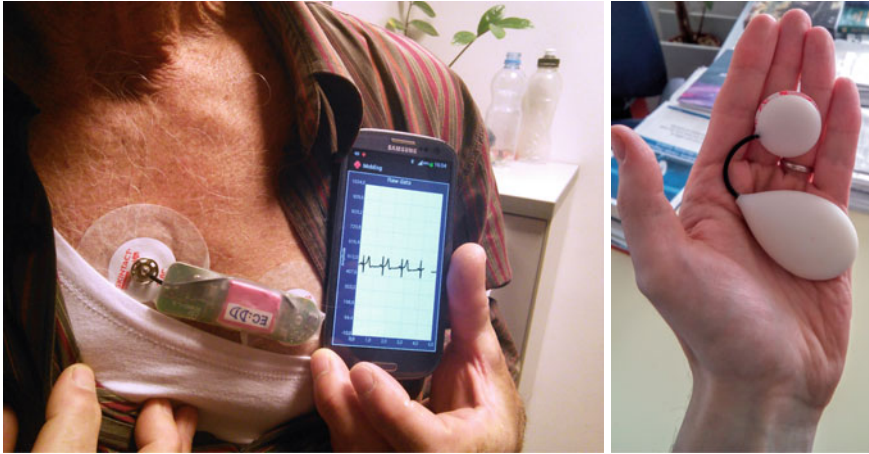


Fig. 2.5 An early prototype of an ECG body sensor connected through low-power Bluetooth with a mobile phone (*left*) and a near-to-market ECG sensor in a flexible design (*right*)

2.3.2 Positioning of an ECG Body Sensor

It can be expected that the body sensor ECG differs significantly in different positions. Some positions are better for monitoring atrial activities, particularly, morphologies of the P wave and types of arrhythmic events. The existing knowledge for the interpretation of the conventional 12-lead ECG is of limited use in the case of a wireless body sensor, because the latter neither has a fixed position nor is its output comparable with any standard lead. However, the existing knowledge is still useful for heart rhythm monitoring. Because the ECG body sensor gives a close look on the heart, it offers a novel type of electrocardiographic data that requires further research for proper interpretation [14].

Based on our experience from MEEG measurements and on the investigation of BSMs and their gradients (see the explanation and Fig. 2.4 in the previous section), in the following, we propose some positions for the ECG body sensor, which give adequate results in the analysis of heart rhythm [15]. The positions are encoded with a simple labeling scheme shown in Fig. 2.6. Note that all positions are near the heart atrium to better capture the P wave. The reference point of the scheme is on the sternum, 5 cm superior to the xiphoid. To establish unambiguous labels of ECG sensor positions, four standard letters: L (left), R (right), S (superior) and I (inferior), are used. The first letter denotes the position of the positive electrode relative to the sternum, L or R. The positive electrode is located under the larger half of the sensor. We suppose that the sensor can be translated in steps of about 5 cm (or half of the sensor length) in the horizontal direction (towards L or R), which is denoted with the second letter. Any translation in the vertical direction, towards S or I, again

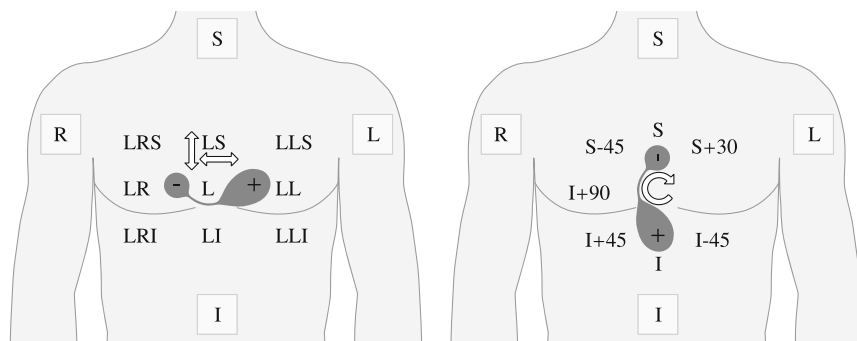


Fig. 2.6 Labeled positions of the sensor obtained by translation in a 5 cm mesh (*left*), and labeled positions of the sensor obtained by rotation for a selected angle in degrees (*right*)

for about 5 cm, is denoted with the third letter. Note that positions with nil or only one translation are labeled with less letters; e.g., position LL is at the level of the reference point, moved to the left for 5 cm.

The position of the sensor shown in the left part of Fig. 2.6 is labeled with L, because the larger half of the sensor (the positive electrode) is left from the sternum and the sensor center is above the reference point—no translation has been applied. The standard ECG leads V1 and V2 are 5 cm towards S, and the corresponding position of the ECG sensor that would be placed in the positions of the V1 and V2 electrodes is labeled with LS. If the sensor is moved from the reference point 5 cm towards I, the sensor position would be labeled with LI or LLI, if it is positioned more to the left. The sensor position above the right atrium and with the positive electrode directed to the left is labeled with LRS. By analogy, the initial L can be replaced with R, if the positive electrode of the ECG sensor is placed on the right side of the reference point, e.g., mirrored around the transfer axis. In this case, the measured signals are reversed in amplitudes if compared with the signals obtained in the positions labeled with the initial letter L.

Alternatively, the ECG sensor can be rotated around its center, in steps of about 45° with the clockwise direction (from the right to the left) regarded as the positive one. In these cases, the first letter, S or I, denotes the position of the positive electrode relative to the reference point. The second place in the label is reserved for the + or – sign and the angle in degrees, denoting the direction and the amount of rotation, e.g., I+45 or I–45, which means that the sensor is rotated from the vertical position with inferior positive electrode for 45° in the positive or in the negative direction, respectively. Again, the initial letter I can be replaced with S, which results in mirrored sensor positions. The labeled positions of the sensor obtained by rotation are shown in the right part of Fig. 2.6. The presented sensor position is labeled with I, because the positive electrode is below (inferior to) the reference point and no rotation has been applied.



Fig. 2.7 ECG sensors fixed with self-adhesive electrodes in the positions LI (*left*) and I (*right*)

Two ECG sensors fixed with self-adhesive electrodes, at the often used positions labeled with LI and I, are shown in the left and the right part of Fig. 2.7, respectively.

Sometimes the ECG sensor cannot be positioned in any of the defined places, because of anatomical or other reasons, such as a surgery wound, furriness, etc. In such cases, one can use modified positions, labeled more precisely with additional letters and numbers. For example, if the ECG sensor is moved from the position I+45 towards the right for 5 cm, its label will be I+45R5, or if the ECG sensor is moved from the position LLS further to the left for 3 cm and up for 2 cm, its label will be LLSL3S2. Note that the rotation step could be also finer than 45° . Any additional characters, however, make the positioning labels more complex. Therefore, they will be used only in some special cases or when higher accuracy of the ECG sensor positioning is needed.

It is evident that the proposed notation results in several equivalent positions, such as L and S+90, or S-45 and I+135. There are also several mirrored positions, such as S and I, or S-45 and I-45, that just provide inverted signals and amplitudes. In any case, while the proposed labeling scheme can be useful in in-depth analysis of the heart rhythm, it can become too complicated for users. They most probably would prefer a short list of predefined, possibly graphically presented positions, from which they can choose before the measurement directly in the mobile application. In each of the presented measurements, we therefore inserted also a schematic graphical presentation of the ECG sensor position used for the particular measurements.

The ECG signal segments obtained when placing the ECG sensor in the nine positions from the left part of Fig. 2.6 are shown in Fig. 2.8. Note that all the signals are accurate enough for a reliable detection of all characteristic ECG waves, but the largest signals have been measured in the positions L, LRI and LI. The P wave is clearly visible in all positions except in LLS.

Figure 2.9 shows four ECGs recorded with the ECG sensor in the positions I+135, I+90, I+45 and I, as labeled in the right part of Fig. 2.6. Note that all four signals are accurate enough to determine all ECG waves and the heart rhythm. The signal from the position I+135 can be labeled also with S-45, which is an equivalent sensor position. The signal from the position I+90 is in fact the inverted signal from the mirror position L, and can also be labeled with R.

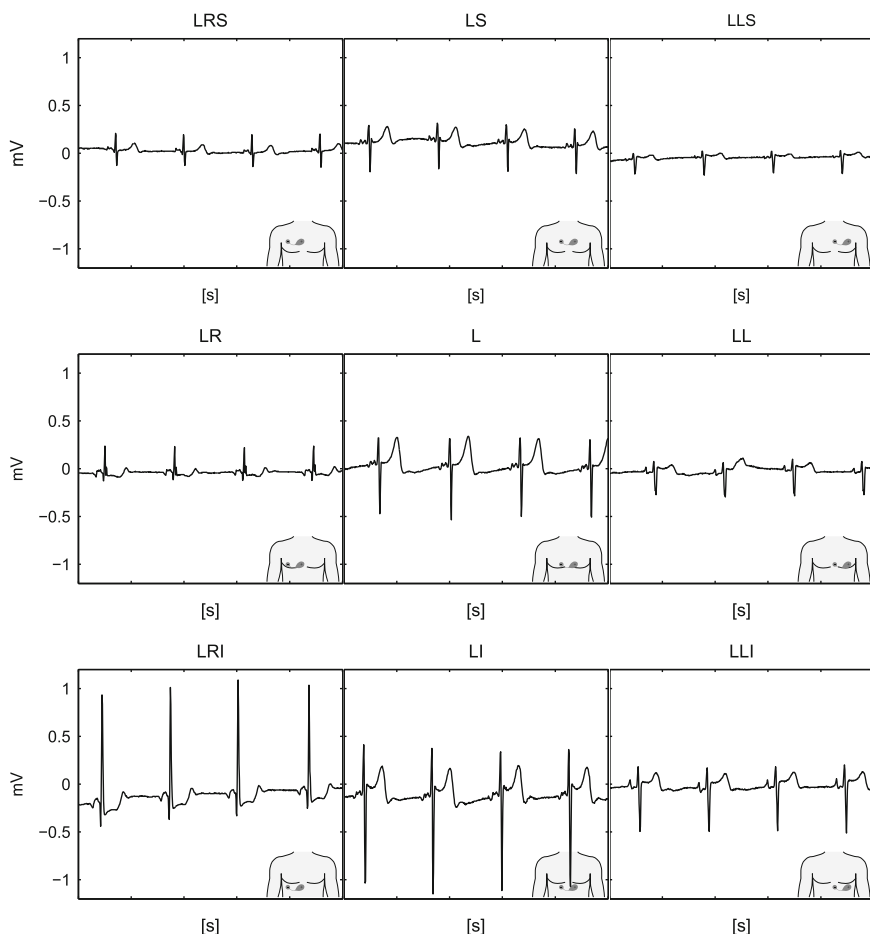


Fig. 2.8 Raw ECG signals obtained from the ECG sensor in the positions shown in the left part of Fig. 2.6

The sensitivity of the ECG body sensor is demonstrated with the recorded abdominal ECG (AECG) in Fig. 2.10. Note that the scale of the graphs is increased because of small signals. The AECG in the left part of Fig. 2.10 was recorded with the ECG sensor placed on the left part of the abdomen at the level of the umbilicus of the same person as in the recordings in Figs. 2.8 and 2.9. Note that the amplitude of the AECG signal is about 0.2 mV, which is significantly smaller than in the previous examples. Therefore, the recording can only suffice for the detection of the heart rate.

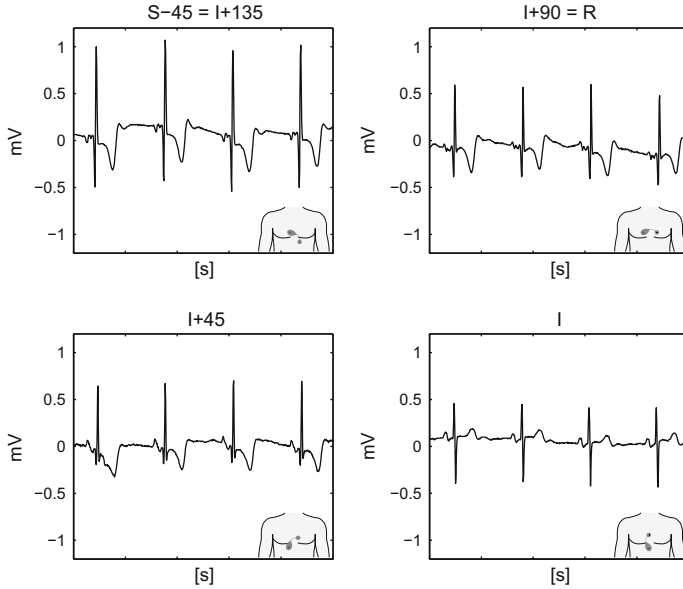


Fig. 2.9 Raw ECG signals obtained from the ECG sensor in four positions shown in the right part of Fig. 2.6

The AECG can be used also as a non-invasive method for monitoring the cardiac activity of a fetus. A complementary method is the detection of fetal heart rate with an ultrasound. For comparison, the right part of Fig. 2.10 shows an AECG with a fetal ECG (FECG) recorded in the fifth month of pregnancy. The sensor was positioned in the center of the abdomen, 5 cm below the umbilicus. The gain of the input amplifier was further increased for a factor of 4.7. The fetal ECG with heart rate of 150 beats per minute (BPM) is superimposed to the mother's AECG with heart rate of 62.5 BPM. Since the fetus is very small, its ECG signal measured on the abdomen during pregnancy has an extremely small amplitude, significantly smaller than the amplitude of the mother's AECG. Therefore, the scale of the graph is further increased. Note that in the fifth month of pregnancy, the size of the fetus' left heart ventricle is only about 15 mm [16]. The AECG peak-to-peak QRS amplitude is approximately $40 \mu\text{V}$, while the QRS amplitude of the FECG is about $15 \mu\text{V}$. The recordings demonstrate the remarkable potential of the ECG body sensor for AECG measurements. The interference from the power grid is not present in the signal, which is crucial for further analysis.

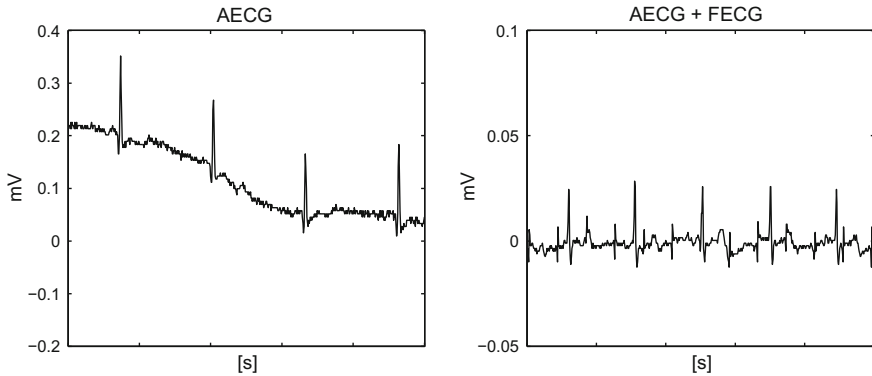


Fig. 2.10 Raw AECG signal obtained with the ECG sensor positioned on the left part of the abdomen at the level of the umbilicus (*left*), and AECG recorded in the fifth month of pregnancy with the sensor positioned in the center of the abdomen, 5 cm below the umbilicus (*right*)

2.3.3 Multiple Body Sensors

So far we have demonstrated the use of a single ECG sensor placed on different locations in the vicinity of the heart. To acquire more information, two sensors, each in a different position, can be used for simultaneous measurement of ECG. Such an approach could be beneficial for better detection of the propagation direction of depolarization waves and consequently for detailed study of the excitation areas. However, new knowledge is needed for proper interpretation of such ECG measurements.

As an example, two concurrently measured ECGs from two independent sensors are shown in the left part of Fig. 2.11. For easier comparison, the measured ECG signals are shown in two graphs vertically separated by 1 mV. The upper graph was obtained from the ECG sensor in the position I+30, while the lower graph from the position I-30. The actual positions of both sensors are shown on the photo in the right part of Fig. 2.11. We see that the morphology of the P waves has changed after the third beat, which could indicate a shift between two atrial excitation focuses. Based on the signals and the knowledge about sensors' positions, an expert electro physiologist could determine the paths of depolarization fronts and consequently the locations of both focuses.

If we further increase the number of sensors, e.g. to three, and place them on appropriate positions, the acquired information can be used for an accurate synthesis of the standard 12-lead ECG. This important topic is described in more detail in Chap. 5.

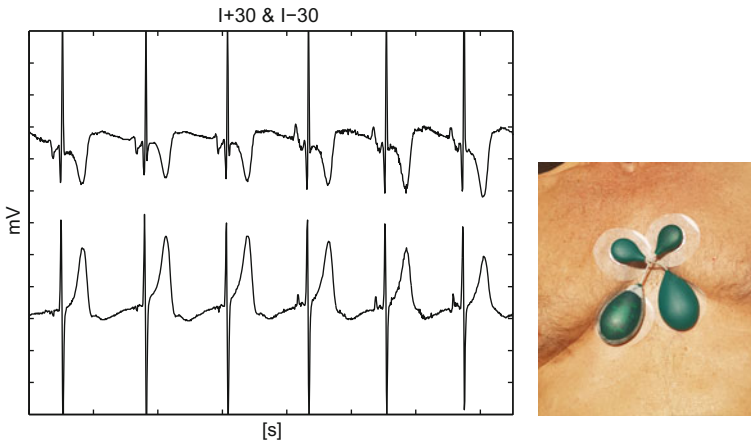


Fig. 2.11 Concurrent measurements from two sensors in the positions I+30 (*graph above*) and I-30 (*graph below*) are shown on the *left*; a photo of the ECG sensors fixed on the body is shown on the *right*

2.4 Multi-functionality of Body Sensors

Hand watches could be historically regarded as the earliest wearable sensors, because they originally provided the timekeeping function. Today, smart watches are available, equipped with sensors able to measure vital signs and with a miniature computer that can analyze the acquired data and communicate with the users and their social networks. The classic hand watches have become so popular because of the beneficial data which they provide, because of their personalized formative design and because of their simple usage, in spite of the complicated mechanism inside. The habit of wearing two hand watches simultaneously, however, has never become popular. It seems that most users, if not seriously stimulated by urgent needs, are ready to wear just a single sensor.

Regarding ECG body sensors, the following aspects have to be considered. The first aspect, related to the implementation of ECG body sensors, is the proximity of the two electrodes that aim to measure a body surface potential difference, which can be measured only if both body electrodes are electrically connected with a data acquisition system. The proximity of the electrodes is important in the context of body sensors because the users have to consider both electrodes as a single wearable unit.

The next aspect, related to the mobility and non-obtrusive use, is the ability of wearable sensors to act as wireless units, which substantially improves their usability and acceptability by the users. However, a lot of work remains to be done in order to select the correct balance between the complexity of the communication protocols, the ability for local signal processing, memory requirements, and the power consumption related to the autonomy of the sensor.

Finally, from the aspect of multi-functionality, sensors that measure the ECG potential difference on the body surface should also provide information on other vital functions, either directly (e.g., for muscular activity, skin resistance, movement, skin temperature, humidity and light) or indirectly (e.g., for respiration), by a customized analysis of the ECG signal. The following subsections present some initial results supporting the proposed multi-functionality approach and the fusion of the measured data for more reliable diagnoses.

2.4.1 Muscular Activity

Surface electromyography (sEMG) is an established non-invasive method for assessing the skeletal muscular activity. If the sensor is placed in the vicinity of the heart, the sEMG signal is superimposed on the ECG and is usually regarded as an unwanted signal disturbance. This is usually the case when one is primarily interested in measuring the heart activity. If the sensor is placed on a specific muscle, however, it can act as a regular sEMG sensor. By using the sensor measurements as an input to a dedicated software, specific muscular activity could be detected and interpreted.

We have performed an experiment where the ECG sensor was placed on the right-hand biceps brachii muscle of a male subject, following the SENIAM recommendations [17] (see left part of Fig. 2.12). A measuring protocol, based on the variation of the time intervals and the muscular load, is presented in Table 2.1.

The corresponding rectified sEMG signal (in blue), sampled at 125 Hz, with marked intervals defined by the measurement protocol from Table 2.1, is shown in the right part of Fig. 2.12. The red graph is the amplitude envelope estimated by the “EMG amplitude estimation toolbox” described in [18]. This toolbox implements a six-stage algorithm for sEMG amplitude estimation: noise filtering, whitening, multiple-channel combination, demodulation, smoothing and re-linearization. From Fig. 2.12, it is clearly visible that high amplitudes of the measured sEMG correlate well with high muscular loads.

Table 2.1 Muscular activity—sEMG measurement protocol

Interval name	Duration (s)	Description
none	0–30	Movement of fingers
a	30–40	Fast lift of 4 kg weight
b	40–65	Slow lift and hold of 4 kg weight
c	65–80	Slow lift and hold of 6 kg weight
d	80–90	Slow lift and hold of 6 kg weight
e	90–110	Two slow lifts of 12 kg weight

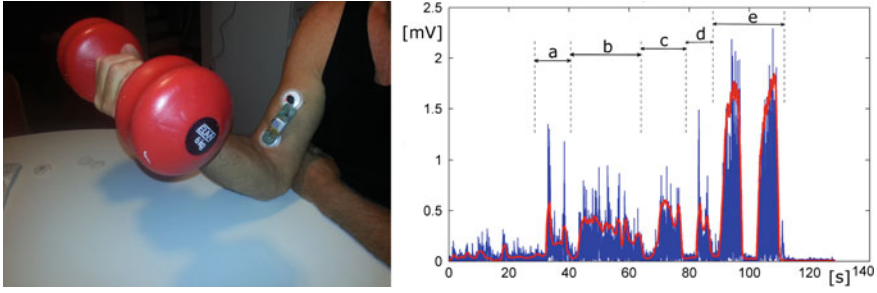


Fig. 2.12 Experimental setup for recording biceps brachii sEMG (*left*). The sEMG measurement obtained in the experiment defined in Table 2.1 (*right*)

One possible application of the sEMG obtained by a wireless ECG body sensor is in physiotherapy. A muscle activation is monitored using sEMG, so that users percept auditory or visual stimulus for their activity (biofeedback). Another application is in the monitoring of sport activities. The obtained sEMGs can be used to assess the force generated by a muscle [19] or the amount of fatigue in a muscle [20]. Additionally, the sEMG obtained by an ECG sensor can be used in combination with other sensors, such as accelerometers, for monitoring the physical activity of specific professionals (occupational bio-mechanics), or for remote exercise monitoring.

An additional potential benefit from sEMG is the ability to detect muscular activities for purposes other than body movement. For example, the breathing rate can be extracted to some extent from a recorded ECG, which is evident from the 20 seconds of raw ECG measurement shown in Fig. 2.13. For this particular measurement, the ECG sensor was placed in the position LI (see Fig. 2.6). The sEMG signal is visible as a low-amplitude noise, superimposed over the ECG signal during four deep inhales. Note that the variation in the ECG amplitude is in a close correlation with the

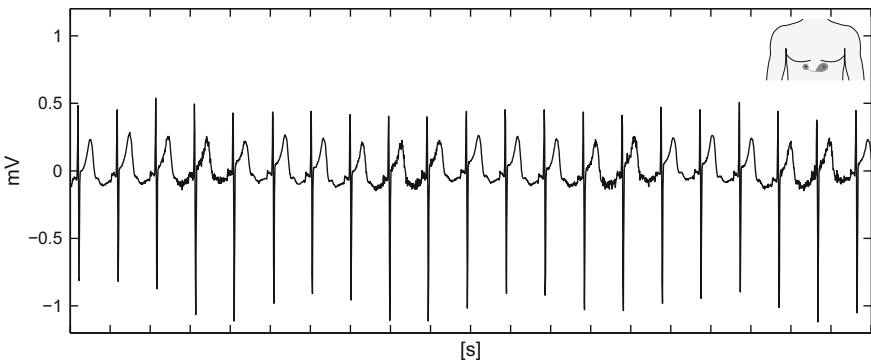


Fig. 2.13 A 20s ECG sensor measurement with a “noise” from the muscular activity during four respiration cycles

sEMG. Such additional information about the respiration could contribute, in combination with other methods, for reliable detection of the respiration rate. The observed amplitude variation is the basis for the technique of ECG-derived respiration, which is described in the next subsection.

2.4.2 *Respiration Derived from ECG*

Breathing is one of the most characteristic vital signs and can reflect the status of a patient or the progression of an illness. The cyclic process that starts with inhale and ends with exhale is referred to as breathing or respiration cycle. The respiratory rate indicates the frequency of breathing and can be obtained from the time between two consecutive inhales or exhales. Any deviations in the respiratory rate can help predict potentially serious clinical events, such as a cardiac arrest, or may suggest that a patient has to be admitted to an intensive-care unit [21].

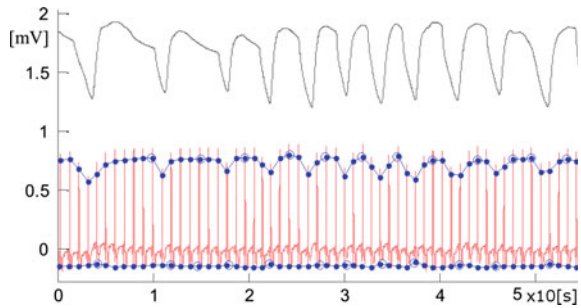
ECG-derived respiration (EDR) techniques [22] are based on two observations. First, the ECG electrodes fixed on the chest move relative to the heart. Second, the transthoracic impedance varies as the lungs fill and empty. Both phenomena influence the amplitude of the recorded ECG and thus a careful analysis of an ECG can be used to derive the breathing rate. Another well-known method of breathing rate derivation is based on the knowledge that the beat-to-beat interval varies primarily due to respiratory sinus arrhythmia (RSA). The heart rate variability (HRV) induced by RSA is more pronounced in young and healthy subjects, which is one of the limitations of this method [23] when applied on older subjects.

In the review paper [24], electrical impedance pneumography across the chest and a photoplethysmogram of a finger were fused to achieve very robust results. The estimation of the breathing rate was still limited by artefacts introduced by movements. Thirteen different algorithms for the detection of sleep apnoea from ECG recordings were analyzed in [25]. The algorithms were based on the frequency-domain features to estimate the changes in the heart rate and the respiration rate. The respiration-related HRV is reduced in the elderly, but the ECG waveform amplitude variability persists regardless of age. Hence, the latter approach could provide better overall performance.

All the above-mentioned approaches for breathing rate derivation are based on wired electrodes and external devices that cannot be considered as a body sensor. It can be expected that the ECG body sensor, placed on the chest near the heart, can reliably estimate the respiration rate by analyzing the QRS amplitudes. The results could be further improved by concurrent measurement of the impedance between the two electrodes.

A simple algorithm for the derivation of the respiration rate can be designed from the following functional blocks: QRS detection, baseline wandering removal, interpolation of QRS amplitudes to obtain the envelope of the respiration-induced variations, resampling of the interpolated QRS amplitudes. The final phase of the algorithm is the detection of the respiration cycles from the re-sampled QRS ampli-

Fig. 2.14 ECG measured with an ECG body sensor (*red graph*) and respiration measured with a thermistor (*gray graph*). All 58 R- and S-peaks (*blue points*) and 11 respiration cycles (*blue circles*) have been correctly detected



tudes variations induced by respiration. QRS and respiration cycles can be detected relatively simply, because of their characteristic periodic variations in amplitudes, which makes this method relatively easy to implement.

An algorithm that can reliably extract respiration rates from variations in the R-peak amplitudes is described and evaluated in more detail in [26]. The principal approach is visualized in Fig. 2.14. The ECG measurement of 53 seconds (red graph) was obtained from a ECG body sensor in the position I according to the notation in Fig. 2.6. At the same time, for validation of the EDR algorithm, the temperature of the inhaled and exhaled air (gray graph) was measured at the nasal exit.

We see that all 58 R-peaks and 58 S-peaks (blue points) have been correctly detected by a QRS detector. By comparing the amplitude of the R-peaks (blue graph) with the temperature of the respiration air, we can see a strong correlation. Eleven respiration cycles are clearly visible as changes of the R-peak amplitudes. However, a false positive respiration cycle nine was identified in the R-peaks variations. Still, a run of the same algorithm on the S-peaks correctly detected all eleven respiration cycles.

A more extensive study published in [26] has identified several sensor positions near the center of the chest which provide good ECG signals for the EDR technique. However, most of the positions shown in Fig. 2.6 can also be used for EDR, which confirms that the measurements from a single ECG body sensor can provide two seemingly independent measurements, i.e., the heart rate and the respiration rate.

2.4.3 Activity Detection

Movements and other activities can be monitored by solid-state inertial sensors, e.g., a 6-degrees-of-freedom unit with 3-axis accelerometer for measuring translation and 3-axis gyroscopes for measuring rotations. Such units are implemented as miniature micro-electro-mechanical systems (MEMS) and can be easily incorporated into the basic wireless ECG body sensor. The sampling rate of an activity sensor depends on the application, but for simple detection of user's movements, which are mostly of a low frequency, it can be kept low to limit the power consumption. Alternatively, the

analysis of activity sensor measurements can be done locally on the sensor and only predefined features, which have reached the specified threshold values, are transmitted over a radio link. When the user is at rest, only Earth's gravity is measured, which can provide information about the sensor's orientation. By a concurrent analysis of ECG and acceleration, a more in-depth and robust analysis of vital functions can be made, which allows for generating also reliable alerts of dangerous states. For example, the maximal heart rate in resting should not be higher than 100 BPM, while during an intensive physical activity it can be as high as 180 BPM or even more. Also, the heart rate cannot increase momentarily and significantly if the user is not active. A potential reason for such an event could be in an emotional stress or a tachyarrhythmia.

We know that an optimal position of the ECG sensor is in the vicinity of the heart, which is not ideal for the classification of all user's movements, but is still acceptable for activity detection [27]. By using a more complex and real-time data analysis on the inertial data, the recognition of the user's activities and detection of falls can be implemented. Simpler data analysis algorithms are based on predictable and robust rules that help to recognize the static states. Machine-learning based classifiers can further recognize movements, e.g. a fall or a jump, for which the rules alone are not sufficient.

Compared to the previously listed applications, where EMG and QRS amplitude variations are superimposed to the ECG sensor signal, reliable activity recognition requires two independent measurements from two inertial sensors, placed in different positions on the body [27]. Because the measurements are performed with separate sensors with asynchronous clocks, an important additional task appears in data analysis, i.e., synchronization of data streams. The synchronization can be accomplished by the analysis of timestamps inserted into the measurement stream at the time of data sampling [28]. The synchronized signals are then segmented and forwarded to the analysis pipeline that is split in two paths. In one path, the segmented data are transformed into feature vectors for the activity recognition module. In the other path, the fall detection module analyzes the accelerator signals for falls. For real-time analysis, the procedures are repeated several times per second, analyzing the last two seconds of the inertial signals. Further details about the algorithm implementation can be found in [29].

2.4.4 Data Fusion for More reliable diagnoses

In the previous sections, we described the design and development route of a wireless bipolar ECG body sensor for long-term monitoring of users' health status. Taking users' feedback into account, e.g. the notion of unobtrusiveness, and respecting the technical limitations, e.g. power autonomy and signal-to-noise ratio, one can develop a small body device able to measure multiple vital and environmental signals.

Based on our previous research, experimental work, feedback from users and medical practitioners, we propose what is in our opinion the optimal solution for mHealth-based long-term monitoring of vital signals:

- Data acquisition should be performed by a single wireless body device comprising of several sensors and thus able to measure several physiological and physical quantities.
- Multiple parameters should be extracted from a single data source whenever possible, e.g., respiration and EMG from the ECG data.
- The sensor should be able to function autonomously for several days, preferably weeks.
- Measurements should not be required to be strictly continuous—their value lies in their long-term character. The users should be able to put the sensor down or wear it only when they feel comfortable wearing it. Likewise, the software for data analysis should be able to gracefully deal with intervals of missing data.
- Sensors should be used for further evidence-based medicine in areas of heart monitoring and diagnostics, optimization of medicament dosage, self-management of health and similar.

An mHealth system based on multi-functional sensors is able to provide complex real-time data streams, composed of fused data that can be efficiently analyzed by advanced data mining and machine-learning algorithms. The main goal behind the data fusion [30] is the ability of making more reliable alerts or diagnoses [31]. However, to be able to efficiently and reliably implement a complex data analytics on fused data, and to evaluate the required storage and computational resources, several aspects should be addressed.

Data synchronization: The streams of measured data are in general not aligned in time, but for data fusion, they should be synchronized. For example, the ECG and acceleration are obtained from independent sensors, which may run at different clocks or have own local analogue-to-digital converters, and are therefore inherently asynchronous. On the other hand, the signals derived from ECG and are superimposed to it are inherently synchronous with the ECG. The wireless transmission is the next step where the synchronization can deteriorate. The sensor data are transferred in consecutive packets, of which some could be—depending on the communication protocol—lost or delayed, e.g. because of network congestion. Several approaches to maintain the synchronism of data are known [32]. We implemented a simple one based on timestamps inserted into each data packet [28]. At the receiver side, based on the known sampling rate determined on the sensor side, the packets are analyzed and the real-time data is reconstructed. In the case of multiple ECG sensors with slightly different sampling clocks, the synchronization between the sensors is maintained on the basis of common events, e.g. R peaks in the ECG signal. Details about the clock synchronization are given in Sect. 2.3.

Communication and storage complexity: The current technological level of low-power radio communication can manage a low-range wireless transmission of data in the range of 10^4 bits/second, which is enough to cover the data transmission

between the wireless body sensor and a smartphone. The data are collected in the smartphone and can eventually be forwarded to a computer Cloud for storage and further analysis, using more powerful existing mobile network infrastructure with no serious restrictions regarding the power consumption. Still, a problem of network congestion can arise in some cases, because of a huge amount of streamed and near real-time data. The accumulated measured ECG data can reach over 10^7 bytes/day, or approximately 0.5 GB/month/user, which is manageable by the current storage technology, even for several thousands of concurrent users and including measures necessary for medical-grade data reliability. The storage of long-term sensor data could be ultimately implemented in a distributed Cloud-based storage system.

Computational complexity: The program code of the data analytics algorithms should run in ultimate mHealth solutions on the local processor in the sensor, on the smartphone, and on a dedicated server or a computer in the Cloud. To be able to manage the response time of the visualization and analytic software in a reasonable frame, possibly in real time, the number of floating point operations per second (FLOPS) must remain proportional to the number of data samples, which could reach 10^4 bytes/second of fused data from a multifunctional body sensor. Assuming that 100 FLOPS are needed for an analysis of each byte, the computational complexity of data visualization and analytics results in 10^6 FLOPS. Additional computing resources are needed for data compression and encryption, which could contribute additional 100 FLOPS/byte. The estimated computational complexity per user is 2×10^6 FLOPS or 2 MFLOPS. It can be further assumed that several phases of data analytics will be implemented on different processors (sensor, smartphone, monitoring center, Cloud) and that each user is equipped with a sensor and a smartphone, with independent measurements and computation that can run concurrently and in parallel. Assuming finally that a contemporary high-performance computer can manage around 50 GFLOPS, it follows that several ten thousands of users' data streams, e.g. 25.000, could be managed by a single dedicated high-performance computer. However, in reality, an overhead will be present, because of input/output data transfer within the computer. Therefore, it seems that a more reasonable estimation is several thousands of users. A bottleneck will certainly remain the assistance of medical experts who must confirm the diagnoses or alerts for each individual user. Further details about software implementation issues are given in the next section.

References

1. Trobec, R., Avbelj, V., Rashkovska, A.: Multi-functionality of wireless body sensors. The IPSI BgD Trans. Internet Res. **10**, 23–27 (2014)
2. Trobec, R.: Computer analysis of multichannel ECG. Comput. Biol. Med. **33**(3), 215–226 (2003)
3. Avbelj, V., Trobec, R., Gersak, B.: Beat-to-beat repolarisation variability in body surface electrocardiograms. Med. Biol. Eng. Comput. **41**(5), 556–560 (2003)

4. De Ambroggi, L., Musso, E., Taccardi, B.: Body surface mapping. In: Macfarlane, P.W., Lawrie, T.D.V. (eds.) *Comprehensive Electrocardiology, Theory and Practice in Health and Disease*. Pergamon Press (1989)
5. Lux, R.L., Smith, C.R., Wyatt, R.F., Abildskov, J.A.: Limited lead selection for estimation of body surface potential maps in electrocardiography. *IEEE Trans. Biomed. Eng.* **25**(3), 270–276 (1978)
6. Gerstenfeld, E.P., SippensGroenewegen, A., Lux, R.L., Lesh, M.D.: Derivation of an optimal lead set for measuring ectopic atrial activation from the pulmonary veins by using body surface mapping. *J. Electrocardiol.* **33**(Suppl), 179–185 (2000)
7. Yamada, T., Fukunami, M., Shimonagata, T., Kumagai, K., Sanada, S., Ogita, H., Asano, Y., Hori, M., Hoki, N.: Dispersion of signal-averaged p wave duration on precordial body surface in patients with paroxysmal atrial fibrillation. *Eur. Heart J.* **20**(3), 211–220 (1999)
8. Gersak, B., Trobec, R., Gabrijelcic, T., Avbelj, V.: Comparison of the ST-40ms isointegral maps prior to and after aortocoronary revascularisation. *Comput. Cardiol.* **24**, 505–507 (1997)
9. Avbelj, V.: Analiza električne aktivnosti srca s pomočjo večkanalne elektrokardiografije [Analysis of the heart's electrical activity by multichannel electrocardiography]. (Doctoral dissertation in Slovene language), Ph.D. thesis, University of Ljubljana, Slovenia (2003)
10. Avbelj, V., Trobec, R., Gersak, B., Vokac, D.: Multichannel ECG measurement system. In: *Proceedings of the Tenth IEEE Symposium on Computer-Based Medical Systems*, 1997, pp. 81–84
11. Boineau, J.P., Canavan, T.E., Schuessler, R.B., Cain, M.E., Corr, P.B., Cox, J.L.: Demonstration of a widely distributed atrial pacemaker complex in the human heart. *Circulation* **77**(6), 1221–1237 (1988)
12. Ferrer, A., Sebastián, R., Sánchez-Quintana, D., Rodríguez, J.F., Godoy, E.J., Martínez, L., Saiz, J.: Detailed anatomical and electrophysiological models of human Atria and Torso for the simulation of atrial activation. *PLOS ONE*, 1–29 (2015)
13. Gorjup, V., Jazbec, A., Geršak, B.: Transtelephonic transmission of electrocardiograms in Slovenia. *J. Telemed. Telecare* **6**(4), 205–208 (2000)
14. Hansen, I.H., Hoppe, K., Gjerde, A., Kanter, J.K., Sorensen, H.B.D.: Comparing twelve-lead electrocardiography with close-to-heart patch based electrocardiography. In: *Proceedings of the 37th Annual International Conference of the IEEE Engineering in Medicine and Biology Society (EMBC)*, 2015, pp. 330–333
15. Puurtinen, M., Viik, J., Hyttinen, J.: Best electrode locations for a small bipolar ECG device: signal strength analysis of clinical data. *Ann. Biomed. Eng.* **37**(2), 331–336 (2009)
16. Sharland, G., Allan, L.: Normal fetal cardiac measurements derived by cross-sectional echocardiography. *Ultrasound Obstetr. Gynecol.* **2**(3), 175–181 (1992)
17. Hermens, H.J., Freriks, B., Disselhorst-Klug, C., Rau, G.: Development of recommendations for SEMG sensors and sensor placement procedures. *J. Electromyogr. Kinesiol.* **10**(5), 361–374 (2000)
18. Clancy, E.A., Morin, E.L., Merletti, R.: Sampling, noise-reduction and amplitude estimation issues in surface electromyography. *J. Electromyogr. Kinesiol.* **12**(1), 1–16 (2002)
19. Disselhorst-Klug, C., Schmitz-Rode, T., Rau, G.: Surface electromyography and muscle force: limits in sEMG-force relationship and new approaches for applications. *Clin. Biomech. (Bristol, Avon)* **24**(3), 225–235 (2009)
20. Cifrek, M., Medved, V., Tonković, S., Ostojić, S.: Surface EMG based muscle fatigue evaluation in biomechanics. *Clin. Biomech. (Bristol, Avon)* **24**(4), 327–340 (2009)
21. Cretikos, M.A., Bellomo, R., Hillman, K., Chen, J., Finfer, S., Flabouris, A.: Respiratory rate: the neglected vital sign. *Med. J. Aust.* **188**(11), 657–659 (2008)
22. Al-Khalidi, F.Q., Saatchi, R., Burke, D., Elphick, H., Tan, S.: Respiration rate monitoring methods: a review. *Pediatr. Pulmonol.* **46**(6), 523–529 (2011)
23. Langley, P., Bowers, E.J., Murray, A.: Principal component analysis as a tool for analyzing beat-to-beat changes in ECG features: application to ECG-derived respiration. *IEEE Trans. Biomed. Eng.* **57**(4), 821–829 (2010)

24. Tarassenko, L., Mason, L., Townsend, N.: Multi-sensor fusion for robust computation of breathing rate. *Electron. Lett.* **38**, 1314–1316 (2002)
25. Penzel, T., McNames, J., Murray, A., de Chazal, P., Moody, G., Raymond, B.: Systematic comparison of different algorithms for apnoea detection based on electrocardiogram recordings. *Med. Biol. Eng. Comput.* **40**(4), 402–407 (2002)
26. Trobec, R., Rashkovska, A., Avbelj, V.: Two proximal skin electrodes—a respiration rate body sensor. *Sensors (Basel)* **12**(10), 13813–13828 (2012)
27. Gjoreski, H., Lustrek, M., Gams, M.: Accelerometer placement for posture recognition and fall detection. In: 7th International Conference on Intelligent Environments (IE), 2011, pp. 47–54
28. Trobec, R., Depolli, M., Avbelj, V.: Wireless network of bipolar body electrodes. In: Seventh International Conference on Wireless On-demand Network Systems and Services (WONS) (2010), pp. 145–150
29. Gjoreski, H., Rashkovska, A., Kozina, S., Luštrek, M., Gams, M.: Telehealth using ECG sensor and accelerometer. In: 37th International Convention on Information and Communication Technology, MIPRO (2014), pp. 270–274
30. Pantelopoulos, A., Bourbakis, N.: SPN-model based simulation of a wearable health monitoring system. *Conf. Proc. IEEE Eng. Med. Biol. Soc.* **2009**, 320–323 (2009)
31. Wilson, S.J., Wong, D., Pullinger, R.M., Way, R., Clifton, D.A., Tarassenko, L.: Analysis of a data-fusion system for continuous vital sign monitoring in an emergency department. *Eur. J. Emerg. Med.* **23**(1), 28–32 (2016)
32. Rhee, I.-K., Lee, J., Kim, J., Serpedin, E., Wu, Y.-C.: Clock synchronization in wireless sensor networks: an overview. *Sensors (Basel)* **9**(1), 56–85 (2009)

Body Sensors and Electrocardiography

Trobec, R.; Tomasic, I.; Rashkovska Koceva, A.; Depolli, M.; Avbelj, V.

2018, XIV, 122 p. 48 illus., Softcover

ISBN: 978-3-319-59338-8